



Zero-Power Sensors for Smart Objects

*John Kimionis, Wenjing Su,
Jimmy Hester, Jo Bito,
Xuanke He, Tong-Hong Lin,
and Manos M. Tentzeris*

Wireless sensors are pervasive today for applications spanning environmental sensing, safety, health, structural integrity, smart homes, and smart cities. Implementations of wireless sensor networks and Internet of Things (IoT) systems have typically relied on power supplied by batteries, which have a limited lifetime and pose the increased burden on users of replacing or manually recharging them to keep devices up and running.

The process of turning things and devices into “smart” objects (e.g., equipping garments with wearable electronics or mounting gas sensors on signs or lamps in a building) has been the subject of considerable research for many years, but powering those smart objects has always been a bottleneck for scalability. New “zero-power” sensor architectures are needed to network massive numbers of objects and move closer to the principles of the IoT.



IMAGE LICENSED BY INGRAM PUBLISHING

John Kimionis (ioannis.kimionis@nokia-bell-labs.com) is with Nokia–Bell Labs, Murray Hill, New Jersey, United States. Wenjing Su (wenjing.su.gatech@gmail.com) is with Google Research, Mountain View, California, United States. Jo Bito (jbit03@gatech.edu) is with Texas Instruments, Dallas, Texas, United States. Jimmy Hester (jimmy.hester@gatech.edu), Xuanke He (xhe53@gatech.edu), Tong-Hong Lin (thlin@gatech.edu), and Manos M. Tentzeris (etentze@ece.gatech.edu) are with the Georgia Institute of Technology, Atlanta, United States.

Digital Object Identifier 10.1109/MMM.2018.2844031

Date of publication: 7 August 2018

Zero-Power Wireless Sensors

Zero-power wireless sensors can be divided in two main categories:

- *all-passive structures* that alter their electrical characteristics according to a sensed variable
- *low-complexity electronics* that parasitically collect energy from external sources.

The latter are of particular interest; they make use of unclaimed energy that may come from environmental sources, such as solar light, or nearby human-built technology, such as radio transmission devices, thus eliminating the need for dedicated powering (Figure 1).

In this article, we present a collection of sensing, powering, and low-power communication components that can be collectively used to realize zero-power sensors. These components have been effectively employed to demonstrate interesting smart-sensor systems, including wearable electronics that parasitically use handheld radio transmissions for power and communication, light-powered sensors for gas safety in buildings, and airborne-powered sensors used in unmanned aerial vehicles (UAVs)/drones over large areas with limited infrastructure. These disruptive proof-of-concept schemes of ambient/parasitic powering will constitute the platform for next-generation deploy-and-forget smart objects and IoT devices.

Sensing

Microfluidic Sensors

Microfluidics uses microchannels/structures to control extremely small amounts of liquid, enabling multiple-liquid analysis and biomedical, chemical, and environmental sensing. Lab-on-chip (LoC) and wireless liquid sensing aim to minimize and simplify the process of liquid analysis, thereby expanding the practice in various industries including distributed health care, food quality monitoring, and environmental detection. Various RF and microwave structures have been used to sense the electrical properties of the test liquids accurately, noninvasively, contactlessly, and labels-free. Using these structures, the liquid content can be detected without any markers or modification; thus, this approach effectively avoids contaminating the samples and saves time as well as effort. Moreover, because the sensing information is read with an RF/microwave signal, real-time monitoring and wireless sensing can be easily realized with RF/microwave sensors. Furthermore, both microfluidics and microwaves feature a miniaturization approach that corresponds well with the LoC concept [1], [2].

Permittivity is one of the most common parameters used in liquid sensing:

- In nature, liquids have a wide permittivity distribution at microwave frequencies [3]–[5], as shown in Table. 1.
- By varying mixing ratios, combinations of two or more fluids can feature a wide range of continuous permittivity change [6], [7].
- Similarly, if any solute is added to the solvent, the permittivity of the solution changes depending on the concentration of the solute [8]. For many liquids (e.g., water), the environmental temperature has a strong influence on the permittivity values [9].

For example, the fat content in milk [10] and fermentation of wines [11] can be easily monitored by the permittivity value; contamination of ground water can be detected by an abnormal conductivity value [12]. Thus, if a device is capable of detecting small changes in permittivity values of a liquid solution by modifying the device's microwave response (frequency, power, or bandwidth), the same technique can be applied in many IoT scenarios such as food-quality monitoring and smart health care (Figure 2).

Resonator-Based Sensors

Resonators have been extensively applied in liquids sensing because the resonant frequency, peak attenuation, bandwidth, or quality factor (Q-factor) of resonators can effectively reflect the complex permittivity of the materials. For a particular resonator, the resonant frequency is determined by the effective inductance and capacitance of the equivalent circuit. Based on the equivalent circuits of microwave structures, the capacitors in the circuits can be tuned by changing the relative permittivity values. Due to the direct relation between the effective capacitance and relative permittivity, an increase in relative permittivity leads to an increase in capacitance and a decrease in resonant frequency.



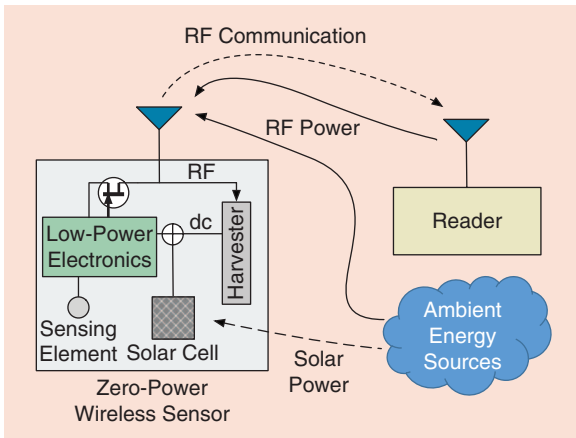


Figure 1. A diagram of a zero-power wireless sensor. The sensor uses ultralow-power electronics and sensing elements, which can be powered by collected RF energy, solar energy, or combinations of the two.

TABLE 1. The permittivity of different fluids at approximately 3 GHz and 300 K [3]–[5].

Name	Permittivity	
	Real part	Imaginary part
Hexanol	3	1
Glycerol	4	0.4
Ethanol	6	7
Water	73	8

For example, a dual-spiral resonator is shown in Figure 3, featuring a relatively high Q-factor while remaining a simple structure. The microfluidic channel is placed on top of the longest slot to achieve better sensitivity due to the locally stronger E-field. Two dual-spiral slot resonators are embedded in the two ground planes of a coplanar waveguide (CPW), so that the transmitted energy over this line will be trapped in the resonator at the frequencies around the resonating frequency, leading to an easy-to-detect bandstop characteristic. Figure 4(a) shows that any $0.4 \log(\epsilon_r)$ change will lead to a

frequency shift greater than one 3-dB bandwidth (10% for low-loss fluids), with the sensor’s resolution relying significantly on the system’s resolution.

The resonant frequency of the bandstop filter shifts by as much as 43.8% when an empty channel is replaced with a water-filled channel; this shows a very high sensitivity compared to state-of-the-art sensors. Figure 4(b) demonstrates the sensor’s ability to distinguish liquid mixtures with different mixing ratios. This sensor is fabricated using a rapid, low-cost biocompatible additive manufacturing technique. The “peel-and-replace” feature allows the sensor to be employed on demand with adjustable sensitivity. Moreover, excellent flexibility is illustrated by the inset photo in Figure 4(a): fewer than 130-MHz resonant frequency shifts and fewer than 1.1-dB insertion loss variations are achieved for down to a 7-mm bending radius [13], which is excellent for liquid sensing in wearable applications.

Dielectric cavity resonators or waveguide resonators have been developed and extensively researched due to their straightforward designs [14], [15]. But they are generally relatively large and require a significant amount of liquid, which conflicts with the LoC principle. Planar resonators—such as the previously mentioned spiral resonator [13] as well as split-ring resonators [16], [17] and stub resonators [18], [19]—have recently been used in microwave sensing. These are much more compact and offer more accurate detection with very small amounts of liquid; thus, planar resonators better correspond to IoT requirements. Multiple resonators working at different resonant frequencies can be integrated on the same platform and could effectively function as chipless RF identifiers (RFIDs) [20] for IoT sensing applications.

Transmission-Based Sensors

Transmission-line sensing topologies have been used in microwave sensing as well, achieving broadband results when very simple microwave structures, such as a CPW line [21], a microstrip line [22], and/or coupled lines [23], are employed. However, the measured data generally require postprocessing, which means

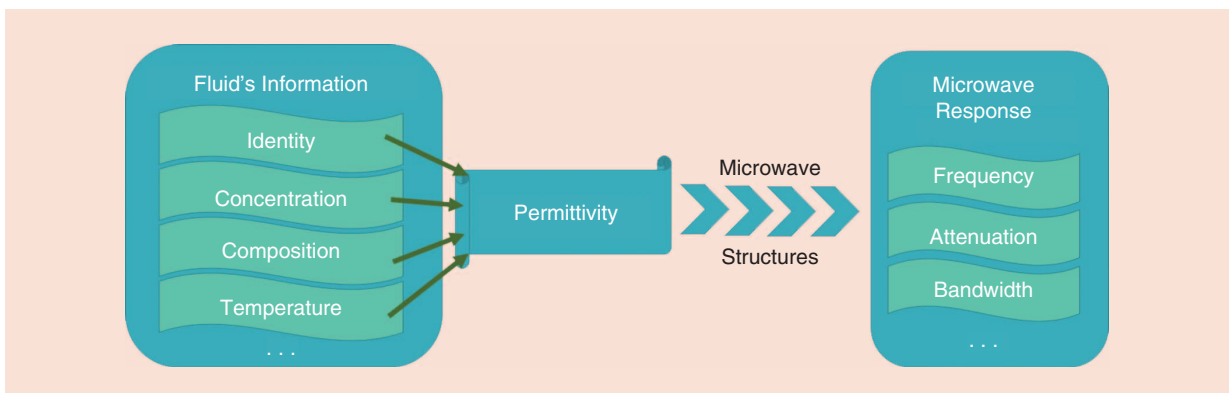


Figure 2. The permittivity sensing mechanism.

the technique is less straightforward compared to that of resonator-based sensors.

By embedding the microfluidic channels into microstrip line configurations, the microstrip impedance will be altered as a function of the channel content. As a proof of concept when this approach is applied to a stepped-impedance, low-pass filter structure, the microwave sensor design in Figure 5(a) is shown. The microfluidic channel is embedded beneath high-impedance microstrip segments to tune the impedance of the microstrip line, as illustrated in the Figure 5(b) inset. The high-impedance segments in the filter are sensitive to the permittivity of the liquid inside the channel; thus, the attenuation of this filter changes for different liquids, as shown in Figure 5(b). This is the first fully inkjet-printed microfluidic sensor, which means it can be fabricated on a single platform and so at an extremely low cost and with great flexibility.

Printed Gas Sensors

Gas-sensing technologies encompass an enormous variety of systems and components, the essential function of which is to translate the presence of targeted chemical analytes into an electrical signal that can be interpreted, processed, and acted upon. In the context of the compact, low-power systems that are the focus of this discussion, the diverse collection of sensors can be winnowed down to a handful of categories (large, power-hungry techniques such as nuclear magnetic resonance spectroscopy are not considered here). With cost, size, and power taken into account, the two main

New “zero-power” sensor architectures are needed to network massive numbers of objects and move closer to the principles of the IoT.

classes of gas sensors best suited for IoT applications can be identified as follows.

- *Amperometric and potentiometric devices* are packaged electrochemical cells, the reactor of which is exposed to the environment in the vicinity of the sensor. The chemistry of the reaction is

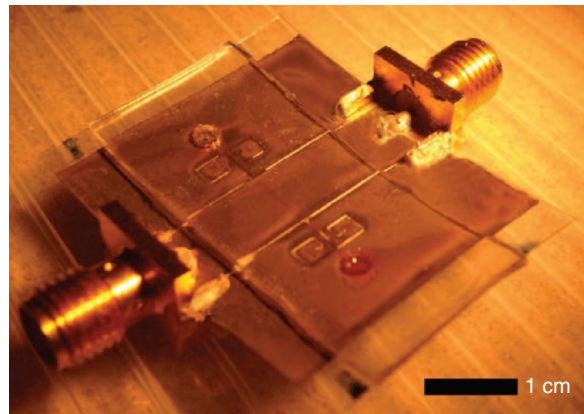


Figure 3. An additively manufactured “peel-and-replace” microfluidic sensor prototype [13].

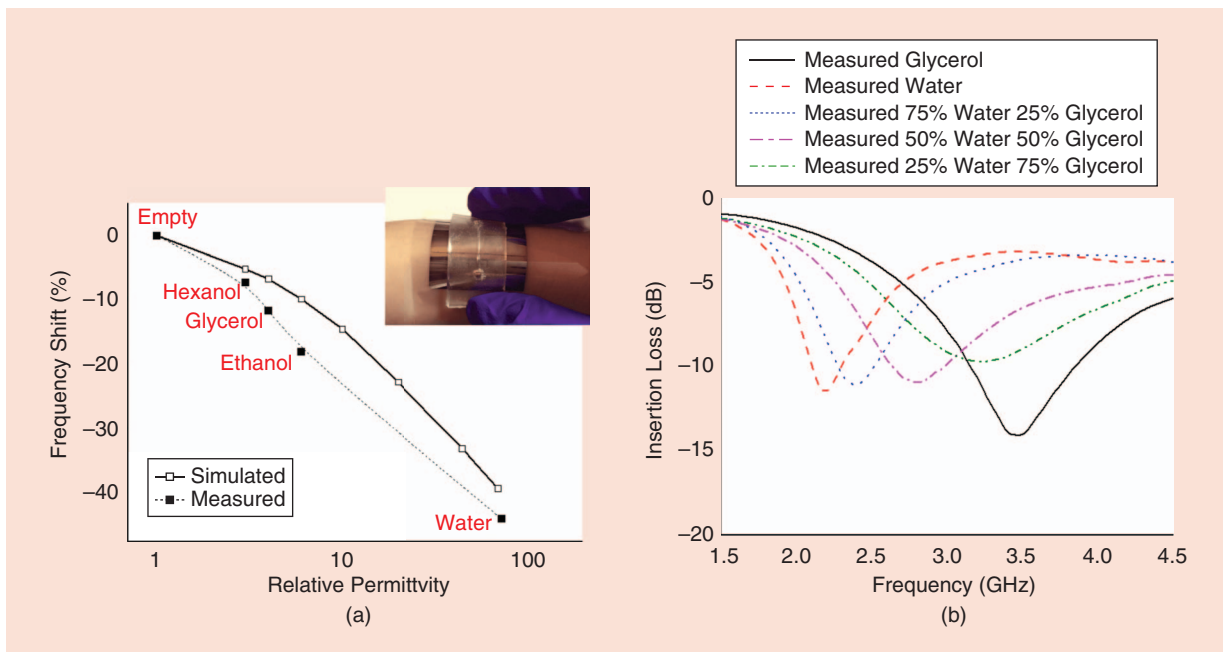


Figure 4. The performance results of the “peel-and-replace” microfluidic zero-power sensor shown in Figure 3. (a) The measured and simulated results of the resonant frequency shift for different relative permittivity fluids inside the channel; the inset photo shows a user wearing the sensor on the wrist. (b) The measured insertion loss values for a glycerol–water mixture, with different mixing ratios inside the channel, which verifies the sensor’s ability to clearly distinguish mixtures with different mix ratios [13].

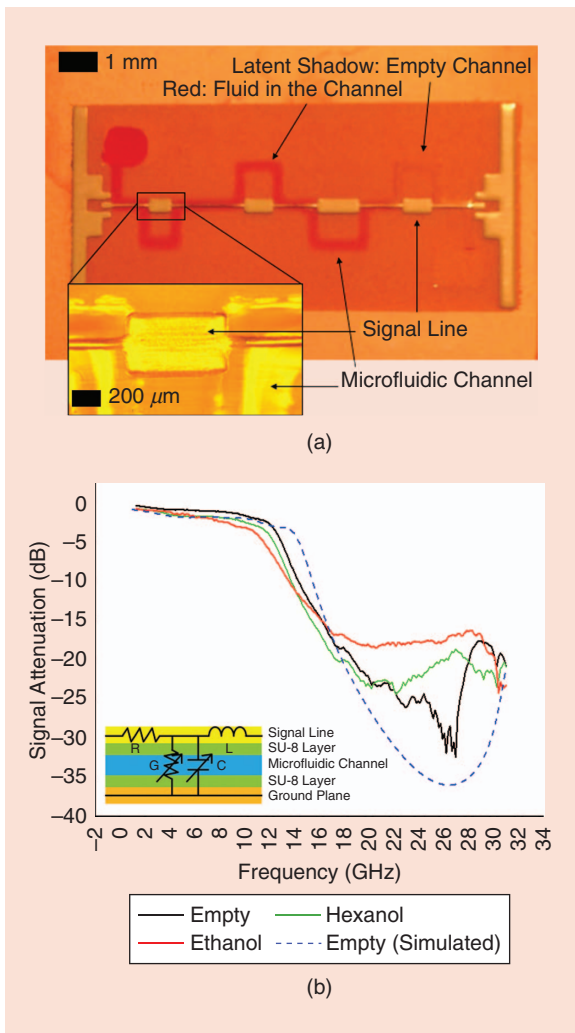


Figure 5. (a) The first fully inkjet-printed microfluidic sensor prototype based on a stepped-impedance low-pass filter. (b) The measured S_{12} values of the sensor, with the equivalent circuit of the microfluidics/microstrip sections shown as an inset [22].

TABLE 2. The state of the art for printed impedometric sensors.

Ref.	Analyte	Lowest Detected Concentration and Associated Sensitivity	Sensing Materials
[27]	H ₂	0.5% at 20 ppm	SWCNT/Pd
[28]	CO ₂	17% at 200 ppm	PPy
[29]	NH ₃	45% at 50 ppm	SWCNT-PABS
[30]	NO ₂	0.5% at 500 ppb	rGO
[31]	CO	2% at 5 ppm	SWCNT-COOH
[32]	CH ₄	1% at 10 ppm	Graphene/PANI
[33]	DMMP	5% at 2.5 ppm	SWCNT

DMMP: dimethyl methylphosphonate; SWCNT: single-wall carbon nanotube; Pd: palladium; PABS: poly(m-aminobenzene sulfonic acid); PPy: polypyrrole; rGO: reduced graphene oxide; COOH: carboxylic acid; PANI: polyaniline.

designed in such a way that the presence of a targeted analyte triggers a redox chemical reaction, the by-products of which are an electrical potential (potentiometric), free electrons, and, thereby, a detectable current (amperometric). In other words, these cells work as batteries whose ability to operate depends on the presence of the targeted gas. Characteristics of this mode include, on the one hand, power-positive operation and, on the other, a limited lifetime. Power-positive operation is especially beneficial for IoT devices because of its ability to wake up nodes upon exposure above a given analyte detection threshold; however, a limit to the total lifetime detection potential of the sensor device (i.e., mote) represents a drawback.

- *Resistometric/conductometric/impedometric sensors* are components the impedance of which changes upon exposure to a targeted analyte. The general term *impedometric* refers to all sensors whose relevant physical property is a complex impedance. More specifically, *resistometric* points to sensors that simply act as chemically modulated variable resistors. Although all representatives of this category have in common the variations of an identical observable (the impedance), this observable can be the product of the modulation of widely differing underlying physical properties, such as Schottky barrier heights [24], intrinsic capacitances [25], [26], or intermolecular electronic orbital coupling.

In addition to differences between the two classes of sensing technologies, a critical distinction in the architecture and, therefore, the ease involved in manufacturing such elements needs to be underlined. Potentiometric/amperometric sensors require the fabrication of an entire electrochemical cell, encompassing two or three electrodes connected to one another via an electrolytic medium (generally a fluid or a gel). As a consequence, these sensors present many challenges for manufacturing in terms of printing techniques alone. In addition, these constraints generally result in large and nonplanar components. By contrast, resistometric elements offer much more lenient manufacturing tolerances and can readily take the shape of fully printed thin-film gas sensors. The current state of the art of such printed elements offers a wide variety of analyte detection capabilities along with high sensitivities, as shown in Table 2.

The differences in the structures and operating principles of the two main classes of sensors outlined here also include important distinctions related to the requirements of their integration context, especially with regard to hybrid RF/low-frequency systems such as the IoT motes that are the focus of this review. While amperometric devices are constrained to low-frequency regimes (as their electrical carriers are low-velocity charged ions), impedometric sensors can readily operate at RF. It is, therefore, possible to

integrate such elements directly into the RF structures, such as passive RFIDs [35]. An example of such a fully inkjet-printed RF element, in the form of a breath sensor, is shown on Figure 6. The sensing component, a film of printed carbon nanotubes interfaced with two inkjet-printed silver electrodes, was characterized and modeled in the 500-MHz–2-GHz frequency range. At those high frequencies, an extremely accurate equivalent electrical model of the element was determined, demonstrating relative component value changes up to 49%, thereby suggesting its sensing ability.

Power

With a few exceptions such as chipless and passive RFIDs, most conventional sensors and IoT devices use active circuits powered by primary batteries for communication and data acquisition. Because batteries can power the devices for only a limited amount of time, one of the most pressing issues is the lack of a sustainable power supply that could enable the operation of such devices autonomously. As the number of IoT devices increases, significant system maintenance cost increases are expected as a result of the need for battery replacement. To avoid these maintenance costs and achieve completely self-sustainable, low-cost, and ubiquitous systems for the IoT, smart cities, and wearable devices, the research community has devoted considerable attention to ambient energy harvesting (EH) and wireless power transfer (WPT) technologies. To maintain effective operation of truly autonomous systems, this technology set uses transducers to harness energy from ambient power sources such as solar, heat, vibration, and electromagnetic waves and stores it in energy-storage components such as secondary batteries and capacitors [36]–[38].

Among ambient energy sources, RF energy is highly attractive because of its almost ubiquitous availability, especially in urban areas, and the low cost and size of transducers [39], [40]. However, compared to the energy density of other sources, that of RF energy is typically very low, so RF energy harvesters cannot directly drive devices that require relatively high power and voltage such as microcontrollers, especially from a cold-start condition (i.e. waking up circuits from deep sleep). Low energy density also results in low RF–dc conversion efficiency, which makes RF EH even more challenging to exploit.

Key emerging applications of the IoT such as augmented/virtual reality devices and electric vehicles/UAVs require relatively high power and repeated battery charging; they thus represent an urgent need for alternative powering methods that can eliminate the physical connection with wires and overcome their short operation time and the inconvenience of wired charging. One solution is WPT using electromagnetic coupling technology, which can wirelessly charge these devices.

As the number of IoT devices increases, significant system maintenance cost increases are expected as a result of the need for battery replacement.

The medical field is one important application area for this technology. For hygienic purposes, the unique ability of high-frequency waves and microwaves to transfer power to sealed devices in a contactless/cable-less way is a major advantage. Furthermore, WPT could have a significant impact in health and biomonitoring applications, virtually eliminating the need for the painful and infection-prone surgical procedures currently necessary for periodic battery replacement by wirelessly charging in vivo implanted electronics. A fundamental challenge arises when the transmit (Tx)–receive (Rx) separation is not constant and the receiver keeps moving. The variable charging distance degrades WPT efficiency, an effect that could be highly problematic, especially as more and more wearable mobile devices that are expected to be charged wirelessly find use in the real world.

The remainder of this section discusses recent efforts in the field of EH and WPT, focusing on wearable and flexible RF EH, WPT, and hybrid RF/solar EH to realize sustainable zero-power sensor IoT systems.

Near-Field Wearable RF Energy Harvesters

Recent improvements in additive manufacturing technology have enabled the fabrication of circuits on flexible materials. Taking advantage of this unique property, it is possible to create wearable RF energy harvesters that, unlike conventional rigid RF energy harvesters, can be comfortably arranged near mobile communication devices. Energy density in the near field of a mobile communication device, such as a two-way talk radio, is much higher than that in the far field; consequently, this is one potential solution for the low output voltage associated with the low energy density of ambient RF EH.

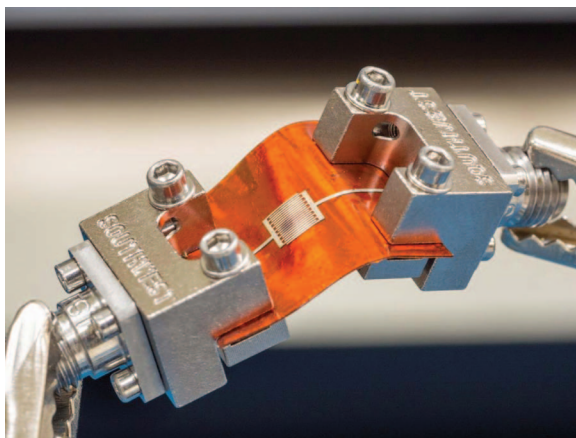
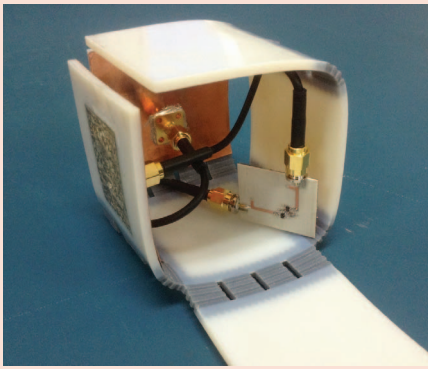
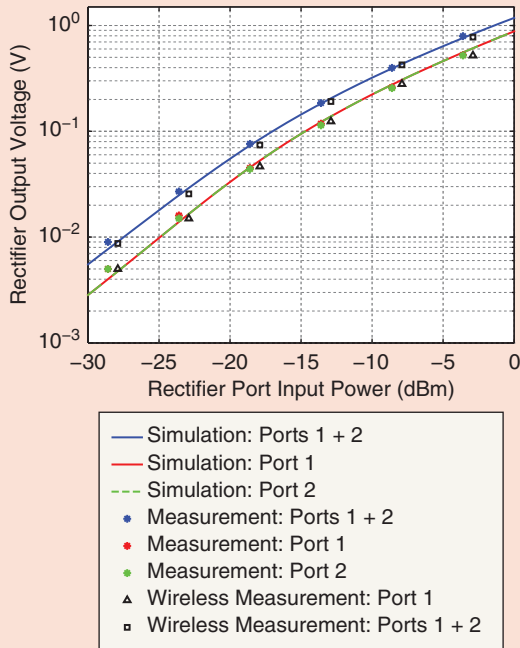


Figure 6. A flexible, fully inkjet-printed breath sensor [34].



(a)



(b)

Figure 9. (a) A 3-D package with orthogonal patch antennas and a dc-combining two-port RF energy harvester. (b) The output voltage of the two-port harvester for one or multiple excited antennas in wired and wireless scenarios [43].

multiple-source, EH-enabled autonomous sensor device. One attractive such combination is hybrid harvesters of ambient solar and RF energies (already been reported in the literature) to increase the available power per unit area because, typically, the energy density of solar energy is much higher than that of far-field RF energy [44]–[46].

High power generation is not the only advantage of using solar cells with an RF energy harvester. One interesting characteristic of solar cells is their inherent ability to generate relatively high voltages above 1 V, even under extremely low-light conditions. As discussed previously, one of the critical limitations for integrating RF energy harvesters in a real system is the low output voltage generated from the harvesters, making it difficult to power conventional ICs. Therefore, using solar cells to power-up ultralow-power dc-dc boost converters makes it possible to significantly increase the sensitivity of RF energy harvesters. Figure 11 shows the custom design of an autonomous hybrid RF/solar-powered sensor device (mote), which consists of a dual-port antenna for both harvesting and communication in the 2.4-GHz industrial, scientific,

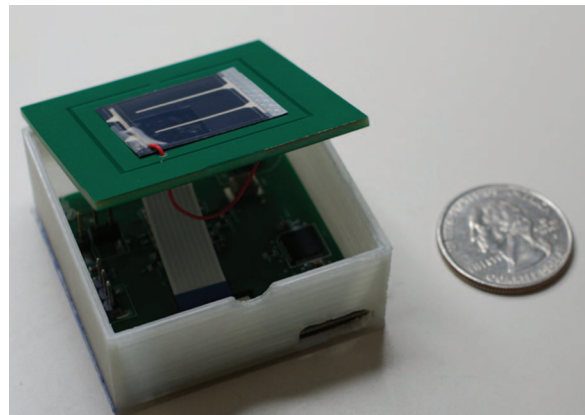


Figure 11. The prototype of an integrated hybrid RF/solar EH system [47].

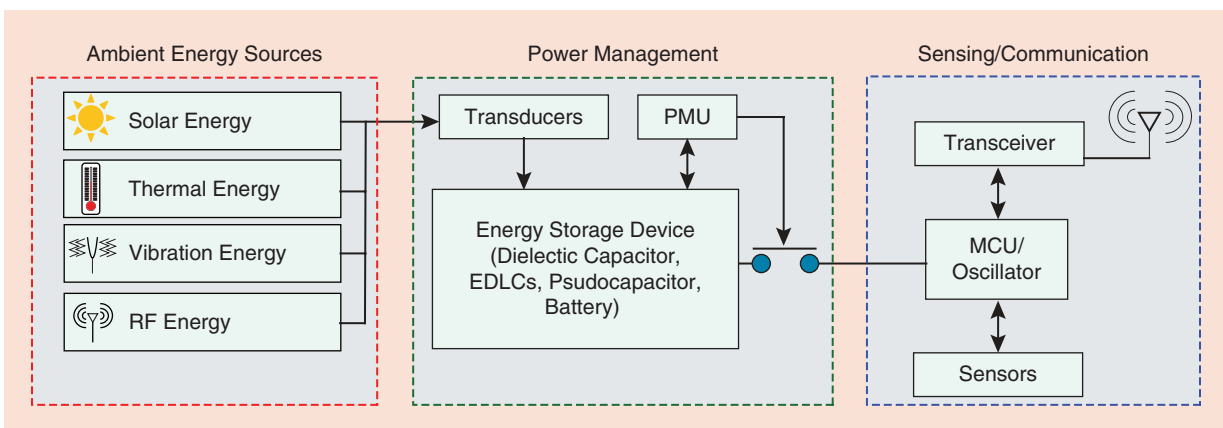


Figure 10. A block diagram of a typical multiform EH-enabled autonomous wireless sensor. EDLCs: electrical double-layer capacitors.

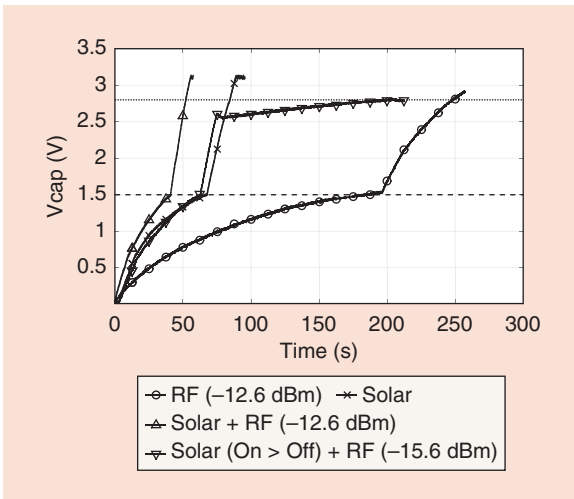


Figure 12. The voltage of the 100- μF capacitor integrated into the bq25504 PMU during charging under different RF and solar conditions: -12.6-dBm RF input power; solar under room lighting conditions; -12.6-dBm RF input power plus solar under room lighting conditions; and -15.6-dBm RF input power plus solar under room lighting conditions until the cold-start mode is completed.

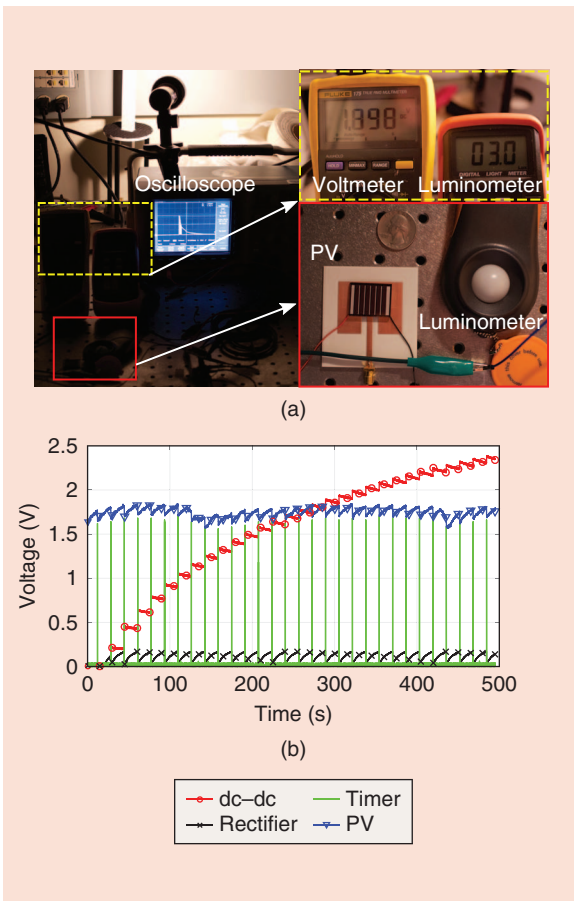


Figure 13. (a) The operation test of the dc-dc converter prototype in a darkroom. (b) The measured output voltage from the dc-dc converter, rectifier, timer, and PV cell during the operation test.

and medical band; a solar cell; a matching circuit; an RF-dc conversion circuit; a bq25504 power management unit (PMU); a capacitor/battery for energy storage; a metal-oxide-semiconductor field-effect transistor (MOSFET) switch; an MSP430 MCU; and a CC2500 transceiver for communications [47].

The output capacitor voltage during the operation of the RF/solar energy harvester is shown in Figure 12. Combining the dc outputs of the solar and RF harvester makes it possible to move beyond the cold-start operation of the bq25504 PMU (which requires high input power), maintaining the operation of the PMU with a lower RF input power level of -15.6 dBm .

As a further extension of this concept, an ultralow-power hybrid RF/solar EH system was designed and fabricated using nanotimers and low-power oscillator ICs. The photovoltaic (PV)-powered timer (which consumes power of fewer than 50 nW) generates short-duration pulse signals with an operational frequency below 0.1 Hz to trigger the operation of a relatively high-power, high-frequency (1–5 μW at 5–90-kHz oscillation frequency) oscillator to minimize the entire system’s power consumption. This low required energy allows the system to operate under even extremely low-light irradiation conditions and without the cold-start issue.

Because the control system requires only 59 nW of power to operate, the output voltage under low-light irradiation is a key factor in the selection of a PV cell. A Panasonic AM-5610CAR 25-mm \times 20-mm amorphous silicon solar cell that exhibits 5.1-V open voltage under one sun irradiation was selected for this work. As depicted in Figure 13(b), the PV cell, which can be mounted on a 2.4-GHz patch antenna, exhibits 1.9 V of open-circuit voltage and supports the operation of the system under 3 lux = 440 $\text{nW} \cdot \text{cm}^{-2}$ irradiation, which is two to four orders of magnitude weaker than office lighting and direct sunlight, respectively. In fact, 3.4 lux is the darkness limit of civil twilight under a clear sky, so 3-lux light irradiation is considered nighttime.

Figure 13(b) shows the output voltage from the dc-dc converter, rectifier, timer, and PV cell during operation under these darkroom irradiation conditions for -20-dBm ambient RF input power. The dc-dc converter successfully charged a 100- μF capacitor to more than 2.4 V within 450 s, with a dc-dc conversion efficiency of 38% and a maximum output voltage of 3 V. The average system output power is 643 nW, which is 10.9 times higher than the minimum required system power. By gradually reducing the RF input power, a net positive output power with output voltage of 1.5 V was confirmed down to -25.0 dBm of RF input power, which is 4 dB and 9.4 dB lower than the state-of-the-art autonomous RF energy harvester [48] and hybrid RF/solar energy harvester [47], respectively.

Communication

Backscatter Low-Power Communication

Typical wireless sensors use active radios for data read-outs. These radios feature power consumption levels on the order of 30–180 mW or more for communication [49]. The main components that govern the power consumption of such radios are the RF local oscillators, mixers, and power amplifiers, which are required to generate and radiate modulated RF signals toward a node/gateway with a receiving radio [Figure 14(a)]. These levels of power consumption significantly limit a wireless sensor's lifetime [50].

Backscatter radio is a promising communication scheme to overcome the challenges of increased power consumption and move toward zero-power sensor implementations. Backscatter/reflection communication has found widespread use in RFID systems due to the low cost of the fabricated tags used to identify objects and commodities as well as to authenticate people [51], [52]. The application of backscatter radio is not limited to static identification codes; it can be used to convey dynamic sensor information as well. A sensor modulates and transmits signals through reflection rather than radiation, effectively minimizing the power required for communication. An active RF source emits signals, and the sensor's antennas reflect these signals with altered phase- and/or amplitude-modulated information. A receiver captures the reflections and decodes the information. Devices that adopt backscatter communication mechanisms have very-low-complexity front ends because the minimal operation for modulation with a reflecting antenna is alternating the load present at the antenna terminals between two values. This can be achieved using a limited number of active devices (transistors, switches, or diodes) that switch on and off, changing the antenna's load-system reflection coefficient [Figure 14(b)]. These minimal front ends feature very low power consumption, from nanowatts to low milliwatts, and can be implemented by all-passive RFID tags [53], semipassive battery-assisted backscatter sensors [54], or custom tags with backscatter modulators and RF energy harvesters [55], [56].

Backscatter radio has been used in commercial RFID tags for identification purposes; here, they are intended to backscatter digital static information saved in their memory (a unique ID code). However, a tag's antenna characteristics (gain, matching, and resonance frequency) can be altered based on a sensed quantity to parasitically modulate dynamic sensor information on the digital backscattered signal. An example of this principle can be found in [57], where the substrate permittivity of a printed RFID tag changes with humidity absorption levels; thus, the tag's resonance frequency shifts in relation to a nominal value. The frequency shift is detected by a tag-performance testing reader and is translated to a humidity-level change. Another

Backscatter radio is a promising communication scheme to overcome the challenges of increased power consumption and move toward zero-power sensor implementations.

approach for sensing-enabled RFIDs can be found in [58]; here, an RFID antenna's impedance changes as a function of the capacitive properties of different liquids that run through a microfluidic channel, so biological tests related to water/ethanol/hexanol can be conducted wirelessly with passive tags.

In [59], a structural-deformation detector was built by using an RFID tag and mapping its variable wake-up power for sensing displacement. Similarly, structural health-monitoring sensors built with frequency-sweeping RFIDs were presented in [60]. Recently, the concept of using multiple inkjet-printed sensing elements on one RFID tag has been introduced: such tags can be interrogated by simple readers built on commodity software-defined radios [61], and these mechanisms enable the use of zero-power smart skins that comprise multiple multimodal sensor matrices.

Apart from using RFID tags to realize zero-power sensors, custom backscatter sensors can be built with improved front-end designs that maintain low-level power consumption and have increased communication performance. Front ends can employ minimal-power RF FETs or complementary MOS switches with low insertion loss for increased backscatter efficiency. Moreover, front-end designs can incorporate RF energy harvesters without compromising the communication

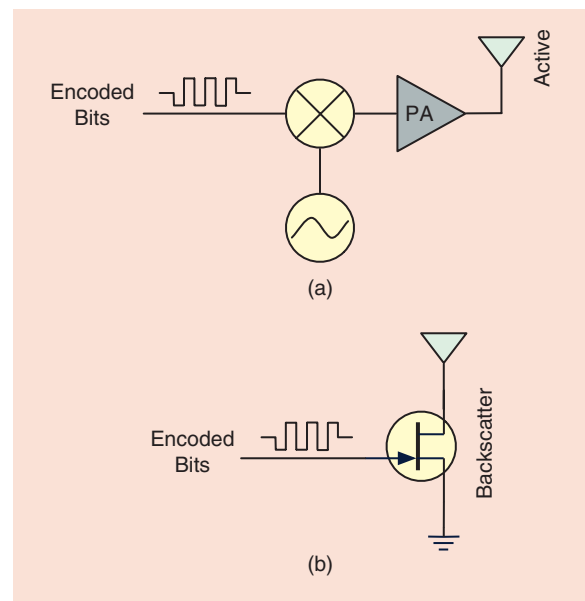


Figure 14. (a) An active radio front end with a power-hungry RF oscillator, mixer, and power amplifier. (b) A backscatter radio minimal front end with a single transistor switch [50].

Although the energy densities of most far-field RF energy sources are relatively low, there are numerous hot spots where RF energy is fairly high; these can generate very high dc voltage and power to power sensors.

efficiency [56]. Backscatter efficiency can be further enhanced on IoT smart sensors with front ends such as reflection amplifiers that amplify and reflect incoming signals from an RF source [62], [63] or pulse-shaping front ends that achieve reduced bandwidth occupancy [55]. Such front ends feature nanowatt to microwatt power consumption levels, and recent work has demonstrated complete wireless sensing systems that include small computational units (microcontrollers), sensing elements, and backscatter modulators, with 350–700- μ W total power consumption [64]. Such power levels can be supported by combinations of RF and solar EH, as described in the “Multiantenna and Hybrid RF/Solar Energy Harvesting” section, for continuous operation with no need for battery/dedicated power sources.

Wearable Backscatter Communication Networks

One key application of the IoT is using wireless sensing networks to construct smart structures such as smart cities and smart skins [66]. RF EH techniques can be used to power these sensor networks. There are many different types of RF energy sources such as ultrahigh-frequency communication, Wi-Fi, and

digital TV signals, especially in urban environments [67], [68]. Although the energy densities of most far-field RF energy sources are relatively low, there are numerous hot spots where RF energy is fairly high; these can generate very high dc voltage and power to power sensors.

A wearable energy-autonomous on-body wireless sensor network system was proposed in [65]; its system architecture is shown in Figure 15. The system is composed of one wearable energy harvester that can perform both rectification and frequency doubling along with multiple wearable and sensing-capable RFID tags with integrated EH circuits. The block diagram of these components is shown in Figure 16.

A handheld two-way talk radio operated at 464.5 MHz is used as the only energy source for three different functions and serves as the foundation for a fully functional sensing system. The first function is to provide energy for sensing-capable RFID tags by integrating EH circuits to harvest energy from the two-way talk radio. A wearable EH circuit (which can be worn on the wrist) is used to enhance the reading range of these sensing-capable RFID tags. Compared with other EH circuits [69], this EH circuit uses both the dc power and second harmonics generated during rectification to provide two additional functions. The RF second harmonic signal output can be used as a wearable mobile carrier emitter to simultaneously illuminate multiple on-body sensing-capable backscattering RFID tags and extend their reading ranges. Meanwhile, the dc power output is used to drive an RF amplifier to further extend the operation range.

A comparison of several wirelessly powered sensor topologies is shown in Table 3, with purely passive RFID

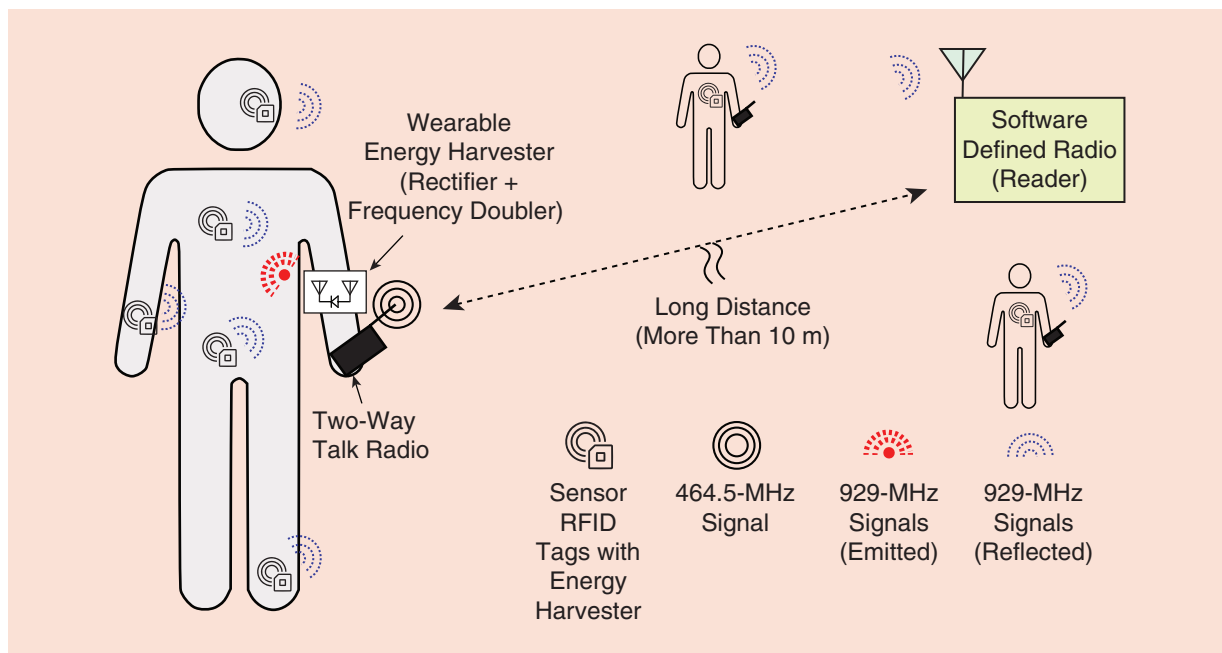


Figure 15. A wearable energy-autonomous on-body wireless sensor network system [65].

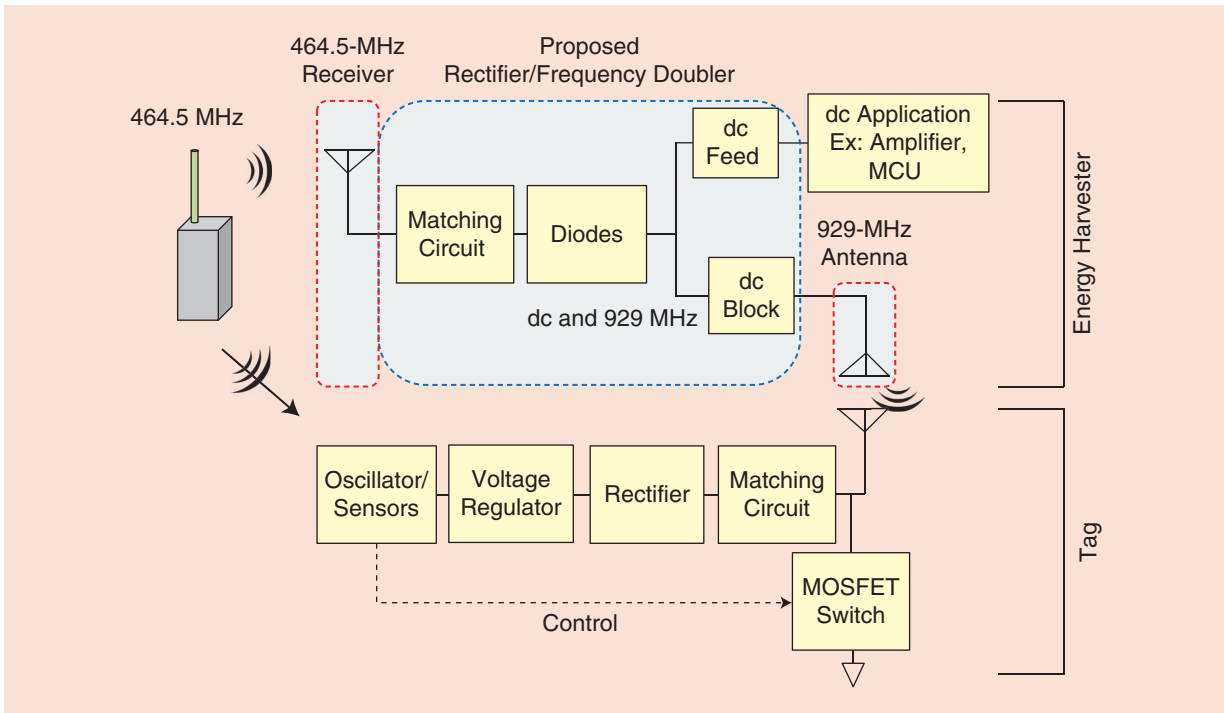


Figure 16. The block diagram of the system in [65].

TABLE 3. A comparison of various RFID tags [72].

Ref.	Operating Frequency	RFID Type	Energy for Tag	Energy for Carrier Emitter	Reading Range (m)
[70]	308 MHz	Active	Battery	n/a	46
[71]	867 MHz	Semipassive + carrier emitter	Battery	Battery	130
[72]	929 MHz	Passive + carrier emitter	Harvested	Harvested	70
[73]	915 MHz	Passive	Harvested	n/a	4
[74]	868 MHz	Passive	Harvested	n/a	6
[75]	900 MHz	Passive	Harvested	n/a	9
[76]	865 ~ 870 MHz	Passive	Harvested	n/a	14
[77]	34.45 GHz	Active	Battery	n/a	11.5

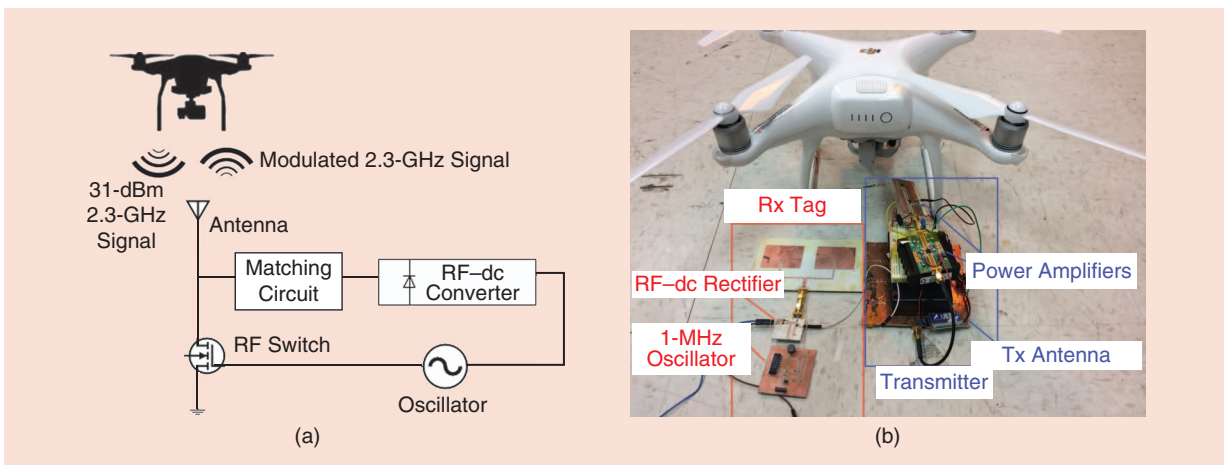


Figure 17. A drone platform for the airborne powering of wireless sensors [78].

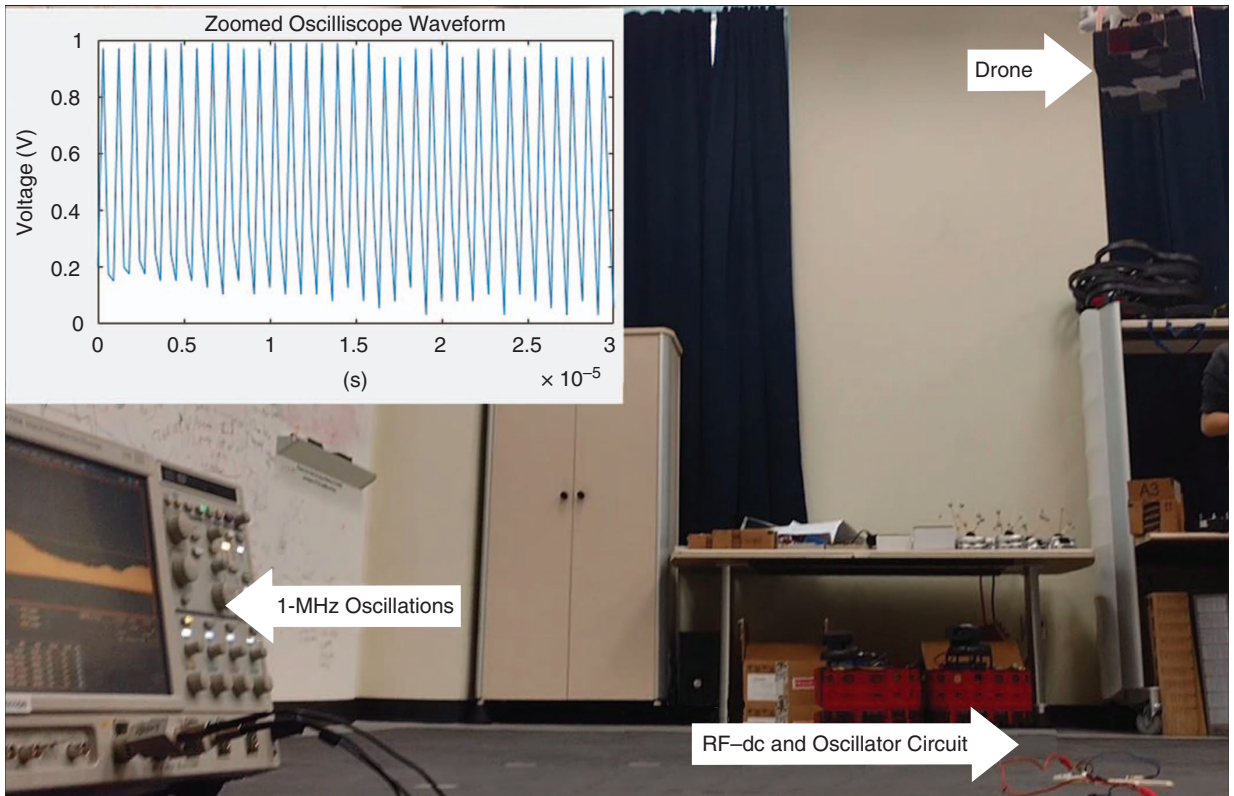


Figure 18. A demonstration of a flying drone at 1.8–2-m height, powering up a 2.3-GHz backscatter sensor. The backscattered 1-MHz signal is captured with an oscilloscope to verify the simultaneous wireless powering and communication operation [78].

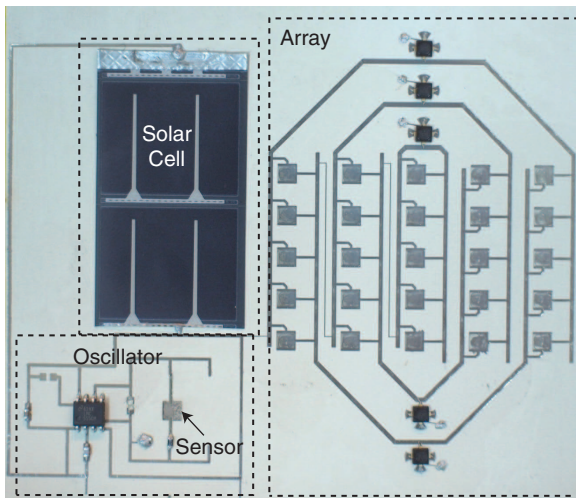


Figure 19. An assembled and printed active Van-Atta reflectarray-based zero-power wireless sensor module [79].

tags achieving reading ranges up to approximately 10 m. The reading ranges of the active RFID tags are more extensive than purely passive ones. For example, a 46-m reading range was achieved in [70]. In [71], a very long (130-m) reading range was achieved using semipassive backscattering tags and carrier emitters. However, batteries are used in both tags and carrier emitters. In [72], a

fully energy-autonomous sensing system with a reading range of 70 m was demonstrated.

Airborne-Powered Backscatter Communication

For remote areas such as national parks or large farms, where the distance to RF base stations is large, it can be cost effective to use drones to deliver power to wireless sensor nodes and simultaneously collect data. In [78], a lightweight, far-field fully customized transmitter and receiver and relatively high-altitude WPT system were developed and experimentally tested. At 2.3 GHz, using a 33-dBm RF power and 9.6- and 8-dB transmit and receive antennas, respectively, as well as factoring in RF-dc conversion efficiency, the measured maximum read distance was approximately 3 m. Figure 17 shows the complete system.

For backscattering, an oscillator was designed for modulation with an oscillation frequency of 1 MHz. RF junction FETs (JFETs) were used as the RF switches, which alternate between a matched state (to power the oscillator) and a short circuit (ground), effectively achieving 180° phase shifting. The switching threshold voltage (V_{th}) for the transistor is as low as 0.4 V, to support harvested power operation. For the oscillator, the use of JFETs and depletion-mode MOSFETs is the best choice due to their 0-V

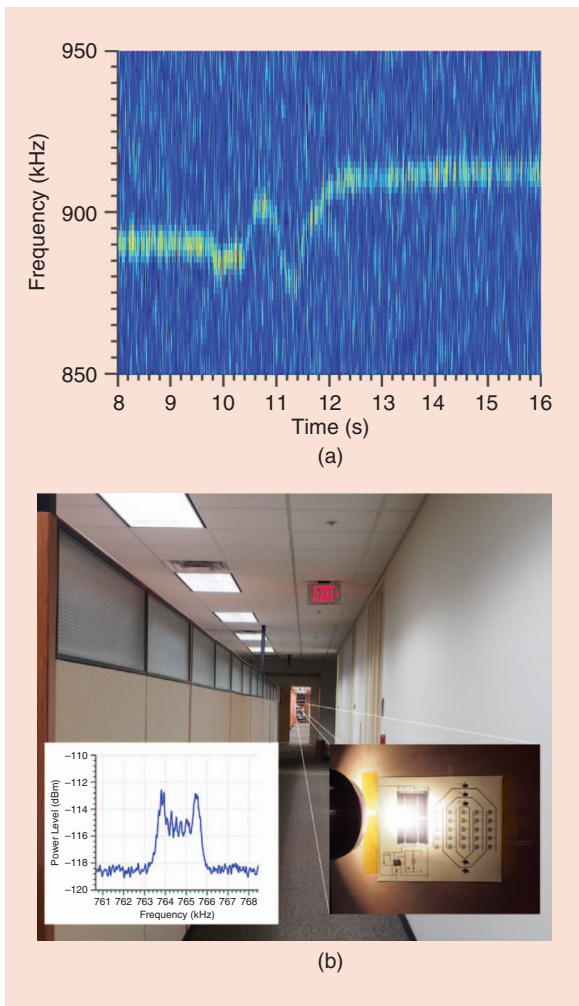


Figure 20. (a) A real-time spectrogram of the wirelessly measured response of the printed Van-Atta reflectarray-based wireless sensing module after exposure to a short illumination of pure anhydrous ammonia. (b) The long-range (80-m) measurement configuration of the Van-Atta reflectarray sensor and the measured intermediate-frequency spectrum [79].

threshold voltage, which reduces the supply voltage and power requirements.

Figure 18 shows the flight test of the drone-integrated transmitter system, along with the 1-MHz oscillation displayed on screen. The oscillator is on, and communication occurs as long as the system is wirelessly powered by the drone. The drone has an advertised 28-min flight time. With the transmitter attached, the flight time is reduced to approximately 20 min, which is enough for practical use with a programmed flight route covering more than 10 km.

Millimeter-Wave Backscatter Sensors

Recently, additive manufacturing has successfully been used to demonstrate millimeter-wave backscatter communication tags, opening the way either to ultra-fast, gigabit-data-rate local-area communication [80] or to long-range, interrogation-angle-tolerant, low-power

sensing [79]. The 28-GHz tag shown in Figure 19 is one such example; it uses a printed cross-polarizing Van-Atta reflectarray that advances the chipless design reported in [81], and [82]. Additional elements include a commercial flexible amorphous silicon solar cell, a low-power 555 timer, and a fully inkjet-printed carbon-nanotubes-based ammonia sensor. In this system, the modulation and encoding of the information are applied by the timer, whose oscillation frequency is related to the resistance of the system's printed resistometric ammonia sensor. A real-time spectrogram of a signal produced during an ammonia detection event is shown in Figure 20(a).

The large aperture of this reflectarray offers high gain, which enabled a reading range of 80 m, as shown in Figure 20(b). This demonstration has opened the door to ultralong-range μ W, flexible, conformal, and printed devices for the IoT.

Looking Forward

Progress on wireless sensor electronics has resulted in power consumption levels in the zero-watt to milliwatt range. Such power consumption levels allow low-power operation of sensing and communication modules, to the point that they can eventually be fully supported by energy sources such as stray/ambient RF emissions or solar light. This effectively eliminates the need for batteries, which have long been deal breakers for long-lifetime operation of wireless sensors. The IoT will move toward a point where sensors and other wireless devices can fully exploit the capability of parasitic powering and operation to achieve high scalability. Pervasive IoT devices will be made possible through the combination of zero-power operation and the low-cost nature of additively manufactured modules.

References

- [1] C. Mariotti, W. Su, B. S. Cook, L. Roselli, and M. M. Tentzeris, "Development of low cost, wireless, inkjet printed microfluidic RF systems and devices for sensing or tunable electronics," *IEEE Sensors J.*, vol. 15, no. 6, pp. 3156–3163, 2015.
- [2] K. Entesari and A. P. Saghari, "Fluidics in microwave components," *IEEE Microw. Mag.*, vol. 17, no. 6, pp. 50–75, June 2016.
- [3] P. Petong, R. Pottel, and U. Kaatz, "Dielectric relaxation of h-bonded liquids. mixtures of ethanol and n-hexanol at different compositions and temperatures," *J. Phys. Chem. A*, vol. 103, no. 31, pp. 6114–6121, 1999.
- [4] R. Nigmatullin, M. A.-G. Jafar, N. Shinyashiki, S. Sudo, and S. Yagihara, "Recognition of a new permittivity function for glycerol by the use of the eigen-coordinates method," *J. Non-Cryst. Solids*, vol. 305, nos. 1–3, pp. 96–111, 2002.
- [5] K. Shibata, "Measurement of complex permittivity for liquid materials using the open-ended cut-off waveguide reflection method," in *Proc. China-Japan Joint Microwave Conf.*, Apr. 2011, pp. 1–4.
- [6] G. Akerlof, "Dielectric constants of some organic solvent-water mixtures at various temperatures," *J. Amer. Chem. Soc.*, vol. 54, no. 11, pp. 4125–4139, 1932.
- [7] R. Behrends, K. Fuchs, U. Kaatz, Y. Hayashi, and Y. Feldman, "Dielectric properties of glycerol/water mixtures at temperatures between 10 and 50 C," *J. Chem. Phys.*, vol. 124, no. 14, p. 144512, 2006.

- [8] R. Somaraju and J. Trumpf, "Frequency, temperature and salinity variation of the permittivity of seawater," *IEEE Trans. Antennas Propag.*, vol. 54, no. 11, pp. 3441–3448, 2006.
- [9] A. Catenaccio, Y. Daruich, and C. Magallanes, "Temperature dependence of the permittivity of water," *Chem. Phys. Lett.*, vol. 367, no. 5, pp. 669–671, 2003.
- [10] W. Guo, X. Zhu, H. Liu, R. Yue, and S. Wang, "Effects of milk concentration and freshness on microwave dielectric properties," *J. Food Eng.*, vol. 99, no. 3, pp. 344–350, 2010.
- [11] A. Garcia, J. Torres, M. De Blas, A. De Francisco, and R. Illanes, "Dielectric characteristics of grape juice and wine," *Biosyst. Eng.*, vol. 88, no. 3, pp. 343–349, 2004.
- [12] M. Arshad, J. Cheema, and S. Ahmed, "Determination of lithology and groundwater quality using electrical resistivity survey," *Int. J. Agriculture Biol.*, vol. 9, no. 1, pp. 143–146, 2007.
- [13] W. Su, B. S. Cook, and M. M. Tentzeris, "Additively manufactured microfluidics-based 'peel-and-replace' RF sensors for wearable applications," *IEEE Trans. Microw. Theory Techn.*, vol. 64, no. 6, pp. 1928–1936, 2016.
- [14] G. Gennarelli, S. Romeo, M. R. Scarfi, and F. Soldovieri, "A microwave resonant sensor for concentration measurements of liquid solutions," *IEEE Sensors J.*, vol. 13, no. 5, pp. 1857–1864, 2013.
- [15] B. Kapilevich and B. Litvak, "Optimized microwave sensor for online concentration measurements of binary liquid mixtures," *IEEE Sensors J.*, vol. 11, no. 10, pp. 2611–2616, 2011.
- [16] H.-J. Lee, H.-S. Lee, K.-H. Yoo, and J.-G. Yook, "DNA sensing using split-ring resonator alone at microwave regime," *J. Appl. Phys.*, vol. 108, no. 1, p. 014908, 2010.
- [17] W. Su, C. Mariotti, B. Cook, S. Lim, L. Roselli, and M. Tentzeris, "A metamaterial-inspired temperature stable inkjet-printed microfluidic-tunable bandstop filter," in *Proc. IEEE 44th European Microwave Conf.*, 2014, pp. 9–12.
- [18] T. Chretiennot, D. Dubuc, and K. Grenier, "Double stub resonant biosensor for glucose concentrations quantification of multiple aqueous solutions," in *Proc. IEEE Microwave Theory and Techniques Society Int. Microwave Symp.*, 2014, pp. 1–4.
- [19] W. Su, J. Cooper, B. Cook, M. Tentzeris, C. Mariotti, and L. Roselli, "Inkjet-printed dual microfluidic-based sensor integrated system," *Proc. IEEE Sensors*, Nov. 2015, pp. 1–3.
- [20] W. Su, Q. Liu, B. Cook, and M. Tentzeris, "All-inkjet-printed microfluidics-based encodable flexible chipless RFID sensors," in *Proc. IEEE Microwave Theory and Techniques Society Int. Microwave Symp.*, May 2016, pp. 1–4.
- [21] S. Liu, I. Ocket, M. Cauwe, D. Schreurs, and B. Nauwelaers, "Sensitivity analysis of broadband on-wafer dielectric spectroscopy of yeast cell suspensions up to 110 GHz," *IEEE Microw. Compon. Lett.*, vol. 25, no. 3, pp. 199–201, 2015.
- [22] W. Su, B. S. Cook, Y. Fang, and M. M. Tentzeris, "Fully inkjet-printed microfluidics: A solution to low-cost rapid three-dimensional microfluidics fabrication with numerous electrical and sensing applications," *Sci. Rep.*, vol. 6, p. 35111, Oct. 2016.
- [23] K. Staszek, I. Piekarczyk, J. Sorocki, S. Koryciak, K. Wincza, and S. Gruszczynski, "Low-cost microwave vector system for liquid properties monitoring," *IEEE Trans. Ind. Electron.*, vol. 65, no. 2, pp. 11665–11674, Feb. 2018.
- [24] S. Heinze, J. Tersoff, R. Martel, V. Derycke, J. Appenzeller, and P. Avouris, "Carbon nanotubes as Schottky barrier transistors," *Phys. Rev. Lett.*, vol. 89, no. 10, pp. 106801, 2002.
- [25] S. Patel, T. Mlsna, B. Fruhberger, E. Klaassen, S. Cemalovic, and D. Baselt, "Chemical capacitive microsensors for volatile organic compound detection," *Sens. Actuators B, Chem.*, vol. 96, no. 3, pp. 541–553, 2003.
- [26] E. Snow, F. Perkins, E. Houser, S. Badescu, and T. Reinecke, "Chemical detection with a single-walled carbon nanotube capacitor," *Science*, vol. 307, no. 5717, pp. 1942–1945, 2005.
- [27] R. Liu, H. Ding, J. Lin, F. Shen, Z. Cui, and T. Zhang, "Fabrication of platinum-decorated single-walled carbon nanotube based hydrogen sensors by aerosol jet printing," *Nanotechnology*, vol. 23, no. 50, p. 505301, Dec. 21, 2012.
- [28] S. A. Waghuley, S. M. Yenorkar, S. S. Yawale, and S. P. Yawale, "Application of chemically synthesized conducting polymer-pyrrole as a carbon dioxide gas sensor," *Sens. Actuators B, Chem.*, vol. 128, no. 2, pp. 366–373, Jan. 15, 2008.
- [29] L. Huang, P. Jiang, D. Wang, Y. Luo, M. Li, H. Lee, and R. A. Gerhard, "A novel paper-based flexible ammonia gas sensor via silver and SWNT-PABS inkjet printing," *Sens. Actuators B, Chem.*, vol. 197, pp. 308–313, July 5, 2014.
- [30] V. Dua, S. P. Surwade, S. Ammu, S. R. Agnihotra, S. Jain, K. E. Roberts, S. Park, R. S. Ruoff, and S. K. Manohar, "All-organic vapor sensor using inkjet-printed reduced graphene oxide," *Angew. Chem. Int. Ed.*, vol. 49, no. 12, pp. 2154–2157, 2010.
- [31] D. Fu, H. Lim, Y. Shi, X. Dong, S. G. Mhaisalkar, Y. Chen, S. Mochhala, and L.-J. Li, "Differentiation of gas molecules using flexible and all-carbon nanotube devices," *J. Phys. Chem. C*, vol. 112, no. 3, pp. 650–653, 2008.
- [32] Z. Wu, X. Chen, S. Zhu, Z. Zhou, Y. Yao, W. Quan, and B. Liu, "Room temperature methane sensor based on graphene nanosheets/polyaniline nanocomposite thin film," *IEEE Sensors J.*, vol. 13, no. 2, pp. 777–782, Feb. 2013.
- [33] J. G. D. Hester, M. M. Tentzeris, and Y. Fang, "Inkjet-printed, flexible, high performance, carbon nanomaterial based sensors for ammonia and DMMP gas detection," in *Proc. European Microwave Conf.*, 2015, pp. 857–860.
- [34] J. G. Hester, M. M. Tentzeris, and Y. Fang, "UHF lumped element model of a fully-inkjet-printed single-wall-carbon-nanotube-based inter-digitated electrodes breath sensor," in *Proc. IEEE Antennas and Propagation Society Int. Symp.*, 2016, pp. 1959–1960.
- [35] L. Yang, R. Zhang, D. Staiculescu, C. Wong, and M. M. Tentzeris, "A novel conformal RFID-enabled module utilizing inkjet-printed antennas and carbon nanotubes for gas-detection applications," *IEEE Antennas Wireless Propag. Lett.*, vol. 8, pp. 653–656, May 2009.
- [36] S. Kim, R. Vyas, J. Bito, K. Niotaki, A. Collado, A. Georgiadis, and M. Tentzeris, "Ambient RF energy-harvesting technologies for self-sustainable standalone wireless sensor platforms," *Proc. IEEE*, vol. 102, no. 11, pp. 1649–1666, Nov. 2014.
- [37] S. Priya and D. J. Inman, *Energy Harvesting Technologies*, vol. 21. New York: Springer, 2009.
- [38] J. A. Paradiso and T. Starner, "Energy scavenging for mobile and wireless electronics," *IEEE Pervasive Comput.*, vol. 4, no. 1, pp. 18–27, Jan. 2005.
- [39] R. J. Vyas, B. B. Cook, Y. Kawahara, and M. M. Tentzeris, "E-WEHP: A batteryless embedded sensor-platform wirelessly powered from ambient digital-TV signals," *IEEE Trans. Microw. Theory Techn.*, vol. 61, no. 6, pp. 2491–2505, June 2013.
- [40] M. Pinuela, P. D. Mitcheson, and S. Lucyszyn, "Ambient RF energy harvesting in urban and semi-urban environments," *IEEE Trans. Microw. Theory Techn.*, vol. 61, no. 7, pp. 2715–2726, July 2013.
- [41] J. Bito, J. G. Hester, and M. M. Tentzeris, "Ambient RF energy harvesting from a two-way talk radio for flexible wearable wireless sensor devices utilizing inkjet printing technologies," *IEEE Trans. Microw. Theory Techn.*, vol. 63, no. 12, pp. 4533–4543, Dec. 2015.
- [42] J. Bito, S. Jeong, and M. M. Tentzeris, "Heuristic passive and active matching circuit design method for wireless power transfer for moving objects," in *Proc. IEEE Wireless Power Transfer Conf.*, Aveiro, Portugal, May 2016, pp. 1–4.
- [43] J. Kimionis, M. Isakov, B. S. Koh, A. Georgiadis, and M. M. Tentzeris, "3D-printed origami packaging with inkjet-printed antennas for RF harvesting sensors," *IEEE Trans. Microw. Theory Techn.*, vol. 63, no. 12, pp. 4521–4532, Dec. 2015.
- [44] M. Danesh and J. R. Long, "Photovoltaic antennas for autonomous wireless systems," *IEEE Trans. Circuits Syst. II*, vol. 58, no. 12, pp. 807–811, Dec. 2011.
- [45] A. Collado and A. Georgiadis, "Conformal hybrid solar and electromagnetic (EM) energy harvesting rectenna," *IEEE Trans. Circuits Syst. I*, vol. 60, no. 8, pp. 2225–2234, Aug. 2013.
- [46] K. Niotaki, A. Georgiadis, and A. Collado, "Dual-band rectifier based on resistance compression networks," in *Proc. IEEE Microwave Theory and Techniques Society Int. Microwave Symp.*, Tampa, FL, June 2014, pp. 1–3.

- [47] J. Bito, R. Bahr, J. G. Hester, S. A. Nauroze, A. Georgiadis, and M. M. Tentzeris, "A novel solar and electromagnetic energy harvesting system with a 3-D printed package for energy efficient Internet-of-Things wireless sensors," *IEEE Trans. Microw. Theory Techn.*, vol. PP, no. 5, pp. 1–12, Feb. 2017.
- [48] K. Gudan, S. Shao, J. J. Hull, A. Hoang, J. Ensworth, and M. S. Reynolds, "Ultra-low power autonomous 2.4 GHz RF energy harvesting and storage system," in *Proc. IEEE Int. Conf. Radio Frequency Identification Technology and Applications*, Tokyo, Japan, pp. 176–181, Sept. 2015.
- [49] M. Johnson, M. Healy, P. van de Ven, M. J. Hayes, J. Nelson, T. Newe, and E. Lewis, "A comparative review of wireless sensor network mote technologies," in *Proc. IEEE Sensors*, Oct. 2009, pp. 1439–1442.
- [50] J. G. D. Hester, J. Kimionis, and M. M. Tentzeris. (2017). "Printed motes for IoT wireless networks: State of the art, challenges, and outlooks," *IEEE Trans. Microw. Theory Techn.*, pp. 1–12. [Online]. Available: <http://ieeexplore.ieee.org/document/7839226/>
- [51] D. M. Dobkin, *The RF in RFID: Passive UHF RFID in Practice*. Oxford, U.K.: Newnes (Elsevier), 2008.
- [52] K. Finkenzerler, *RFID Handbook: Fundamentals and Applications in Contactless Smart Cards, Radio Frequency Identification and Near-Field Communication*, 3rd ed. New York: Wiley, 2010.
- [53] U. Karthaus and M. Fischer, "Fully integrated passive UHF RFID transponder IC with 16.7 μ W minimum RF input power," *IEEE J. Solid-State Circuits*, vol. 8, no. 10, pp. 1602–1608, Oct. 2003.
- [54] E. Kampianakis, J. Kimionis, K. Tountas, C. Konstantopoulos, E. Koutroulis, and A. Bletsas, "Backscatter sensor network for extended ranges and low cost with frequency modulators: Application on wireless humidity sensing," in *Proc. IEEE Sensors*, Baltimore, MD, pp. 1–4, Nov. 2013.
- [55] J. Kimionis and M. M. Tentzeris. (2016, Dec.). Pulse shaping: The missing piece of backscatter radio and RFID, *IEEE Trans. Microw. Theory Techn.*, vol. 64, no. 12, pp. 4774–4788. [Online]. Available: <http://ieeexplore.ieee.org/document/7755817/>
- [56] J. Kimionis and M. M. Tentzeris, "RF tag front-end design for uncompromised communication and harvesting," in *Proc. IEEE Int. Conf. Radio Frequency Identification Technology and Applications*, Tampere, Finland, Sept. 2014, pp. 109–114.
- [57] J. Virtanen, L. Ukkonen, T. Bjorninen, A. Elsherbeni, and L. Sydänheimo, "Inkjet-printed humidity sensor for passive UHF RFID systems," *IEEE Trans. Instrum. Meas.*, vol. 60, no. 8, pp. 2768–2777, 2011.
- [58] B. S. Cook, J. R. Cooper, and M. M. Tentzeris, "An inkjet-printed microfluidic RFID-enabled platform for wireless lab-on-chip applications," *IEEE Trans. Microw. Theory Techn.*, vol. 61, no. 12, pp. 4714–4723, Dec. 2013.
- [59] R. Bhattacharyya, C. Floerkemeier, and S. Sarma. (2009, Apr.). Towards tag antenna based sensing: An RFID displacement sensor, in *Proc. IEEE Int. Conf. Radio Frequency Identification*, pp. 95–102. [Online]. Available: <http://ieeexplore.ieee.org/document/4911195/>
- [60] X. Yi, T. Wu, Y. Wang, and M. M. Tentzeris, "Sensitivity modeling of an RFID-based strain-sensing antenna with dielectric constant change," *IEEE Sensors J.*, vol. 15, no. 11, pp. 6147–6155, Nov. 2015.
- [61] J. Kimionis and M. M. Tentzeris, "Pulse shaping for backscatter radio," in *Proc. IEEE Microwave Theory and Techniques Society Int. Microwave Symp.*, San Francisco, CA, May 2016, pp. 1–4.
- [62] P. Chan and V. Fusco. (2013, Apr.). Full duplex reflection amplifier tag, *IET Microw. Antennas Propag.*, vol. 7, no. 6, pp. 415–420. [Online]. Available: <http://digital-library.theiet.org/content/journals/10.1049/iet-map.2012.0441>
- [63] J. Kimionis, A. Georgiadis, A. Collado, and M. M. Tentzeris, "Enhancement of RF tag backscatter efficiency with low-power reflection amplifiers," *IEEE Trans. Microw. Theory Techn.*, vol. 62, no. 12, Dec. 2014.
- [64] S. N. Daskalakis, J. Kimionis, A. Collado, M. M. Tentzeris, and A. Georgiadis, "Ambient FM backscattering for smart agricultural monitoring," in *Proc. IEEE Microwave Theory and Techniques Society Int. Microwave Symp.*, June 2017, pp. 1339–1341.
- [65] T.-H. Lin, J. Bito, J. G. Hester, J. Kimionis, R. A. Bahr, and M. M. Tentzeris, "Ambient energy harvesting from two-way talk radio for on-body autonomous wireless sensing network using inkjet and 3D printing," in *Proc. IEEE Microwave Theory and Techniques Society Int. Microwave Symp.*, June 2017, pp. 1034–1037.
- [66] L. Atzori, A. Iera, and G. Morabito, "The Internet of Things: A survey," *Comput. Netw.*, vol. 54, no. 15, pp. 2787–2805, Oct. 2010.
- [67] M. Pinuela, P. D. Mitcheson, and S. Lucyszyn, "Ambient RF energy harvesting in urban and semi-urban environments," *IEEE Trans. Microw. Theory Techn.*, vol. 61, no. 7, pp. 2715–2726, July 2013.
- [68] R. J. Vyas, B. B. Cook, Y. Kawahara, and M. M. Tentzeris, "E-WEHP: A batteryless embedded sensor-platform wirelessly powered from ambient digital-TV signals," *IEEE Trans. Microw. Theory Techn.*, vol. 61, no. 6, pp. 2491–2505, June 2013.
- [69] C. R. Valenta and G. D. Durgin, "Harvesting wireless power: survey of energy-harvester conversion efficiency in far-field, wireless power transfer systems," *IEEE Microw. Mag.*, vol. 15, no. 4, pp. 108–120, June 2014.
- [70] L. M. Ni, Y. Liu, Y. C. Lau, and A. P. Patil, "LANDMARC: Indoor location sensing using active RFID," in *Proc. 1st IEEE Int. Conf. Pervasive Computing and Communications*, Mar. 2003, pp. 407–415.
- [71] J. Kimionis, A. Bletsas, and J. N. Sahalos, "Increased range bistatic scatter radio," *IEEE Trans. Commun.*, vol. 62, no. 3, pp. 1091–1104, Mar. 2014.
- [72] T.-H. Lin, J. Bito, J. G. Hester, J. Kimionis, R. A. Bahr, and M. M. Tentzeris, "On-body long-range wireless backscattering sensing system using inkjet-/3D-printed flexible ambient RF energy harvesters capable of simultaneous DC and harmonics generation," *IEEE Trans. Microw. Theory Techn.*, to be published.
- [73] A. A. Kutty, T. Bjorninen, L. Sydänheimo, and L. Ukkonen, "A novel carbon nanotube loaded passive UHF RFID sensor tag with built-in reference for wireless gas sensing," in *Proc. IEEE Microwave Theory and Techniques Society Int. Microwave Symp.*, May 2016, pp. 1–4.
- [74] G. A. Vera, S. D. Nawale, Y. Duroc, and S. Tedjini, "Read range enhancement by harmonic energy harvesting in passive UHF RFID," *IEEE Microw. Compon. Lett.*, vol. 25, no. 9, pp. 627–629, Sept. 2015.
- [75] J. W. Lee and B. Lee, "A long-range UHF-band passive RFID tag IC based on high-Q design approach," *IEEE Trans. Ind. Electron.*, vol. 56, no. 7, pp. 2308–2316, July 2009.
- [76] A. Popov, S. Dudnikov, and A. Mikhaylov, "Passive UHF RFID tag with increased read range," in *Proc. 38th European Microwave Conf.*, Oct. 2008, pp. 1106–1108.
- [77] A. Strobel, C. Carlowitz, R. Wolf, F. Ellinger, and M. Vossiek, "A millimeter-wave low-power active backscatter tag for FMCW radar systems," *IEEE Trans. Microw. Theory Techn.*, vol. 61, no. 5, pp. 1964–1972, May 2013.
- [78] X. He, J. Bito, and M. M. Tentzeris, "A drone-based wireless power transfer ANC communications platform," in *Proc. IEEE Wireless Power Transfer Conf.*, May 2017, pp. 1–4.
- [79] J. G. D. Hester and M. M. Tentzeris, "A mm-wave ultra-long-range energy-autonomous printed RFID-enabled van-Atta wireless sensor: At the crossroads of 5g and IoT," in *Proc. IEEE Microwave Theory and Techniques Society Int. Microwave Symp.*, June 2017, pp. 1557–1560.
- [80] J. Kimionis, A. Georgiadis, and M. M. Tentzeris, "Millimeter-wave backscatter: A quantum leap for gigabit communication, RF sensing, and wearables," in *Proc. IEEE Microwave Theory and Techniques Society Int. Microwave Symp.*, June 2017, pp. 812–815.
- [81] J. G. Hester and M. M. Tentzeris. (2016, May). Inkjet-printed van-Atta reflectarray sensors: A new paradigm for long-range chipless low cost ubiquitous smart skin sensors of the Internet of Things, in *Proc. IEEE Microwave Theory and Techniques Society Int. Microwave Symp.* [Online]. Available: <http://dx.doi.org/10.1109/MWSYM.2016.7540412>
- [82] J. G. Hester and M. M. Tentzeris, "Inkjet-printed flexible mm-wave Van-Atta reflect arrays: A solution for ultra-long-range dense multi-tag and multi-sensing chipless RFID implementations for IoT smart skins," *IEEE Trans. Microw. Theory Techn.*, vol. 57, no. 5, pp. 1303–1309, May 2017.

